Effects of Prandtl number on natural convection in horizontal annular cavities

Samy M. El-Sherbiny and Atef R. Moussa
Mechanical Eng. Dept., Faculty of Eng., Alexandria University, Alexandria, Egypt

The effects of Prandtl number on the laminar natural convection in annular fluid layers between concentric horizontal isothermal cylinders are numerically investigated . The study covered a wide range of the parameters in the ranges $0.01 \le Pr \le 10^3$, $2 \le RR \le 10$ and $10^2 \le Ra \le 10^6$. A computer program is developed to solve the mass, momentum and thermal energy equations with their boundary conditions. The different flow regimes are explained from the generated streamlines and isotherms for different values of the parameters. Local and average Nusselt numbers are given and the distributions of angular velocity and temperature are used to explain the flow regimes. A heat transfer correlation is given which represents all numerical data to within 3.4 %.

تم دراسة تأثير رقم براندل على انتقال الحرارة بالحمل الحر فى طبقات من المائع محصورة بين أسطوانتين أفقيتين متحدتي المحور عند درجتى حرارة مختلفتين . الدراسة العددية شملت التغير فى رقم براندل بين ٠,٠١ ، ١٠^3 ورقم رالى بين ١٠^2 ، ١٠^7 والنسبة بين قطرى الأسطوانتين من ٢ إلى ١٠. وقد تم عمل برنامج حاسب آلى لحل معادلات الكتلة وكمية الحركة والطاقة الحرارية التى تحكم السريان فى طبقات المائع . وقد أستخدمت النتائج الخاصة بخطوط السريان وتوزيع السرعات الزاوية ودرجة الحرارة لشرح تأثير رقم براندل على السريان وانتقال الحرارة وكل من رقم نوسلت الموضعى والمتوسط . تم إستنباط معادلة تمثل جميع النتائج العددية على مدى واسع من المتغيرات المؤثرة وذلك فى حدود إختلاف لا يتعدى ٣,٤٪ .

Keywords: Natural convection, Horizontal cylinders, Annular cavities

1. Introduction

The laminar free convection in fluid annular cavities between two horizontal and isothermal concentric cylinders is an important problem in heat transfer. It is used to simulate a wide range of engineering problems as well as provide a better insight into more complex systems of heat transfer. Numerous applications are found in energy storage, pressurized-gas underground electric transmission cables, liquid metal fast breeder reactors, passive solar systems, cooling of electronic equipment and reactor waste transport and storage.

Several authors have studied the problem. Kuehn and Goldstein [1-3] have reviewed the literature thoroughly. They examined numerically and experimentally the local and average heat transfer coefficients for both concentric and eccentric cylinders. Results were obtained using water and air at atmospheric pressure with a radius ratio ($RR = r_o / r_i$) of 1.25. A Mach-Zehnder interferometer was used to determine temperature distributions and local heat transfer coefficients experimentally. Kuehn and Goldstein [3] presented correlating equations for heat transfer using a conduction boundary layer model. The natural convection in concentric and eccentric horizontal annuli was also investigated numerically by Cho et al. [4] for $Ra < 10^5$ and $1.25 \le RR \le 5$. Grigull and Hauf [5], using a Mach –Zehnder interferometer, presented experimental results of Nusselt number as a function of Grashof and the ratio of the gap width to the diameter of the inner cylinder. They also presented, using smoke dispersion, two-dimensional photographs of the streamlines of the flow fields. Lis [6] pressurized the annulus fluid to achieve turbulent heat transfer. Farouk and Güceri [7] studied both laminar and turbulent flows in annuli of $RR = 2.6$ up to $Ra = 2\times10^7$. The effects of the variation of the fluid properties in the horizontal annulus with temperature were investigated numerically by Hessami et al [8] for air and glycerin in the range (0-50^o C). For air, the effects were negligible but for glycerin, the results indicated a significant

difference in temperature failed between the constant and variable fluid properties assumptions. An experimental study was performed by Hessami et al. [9] for air, glycerin and mercury in the ranges of $0.023 \le Pr \le 10^4$ and $0.03 \le Gr \le 3\times10^6$. The experimental results confirmed the numerical results given in [8]. A parametric study of Prandtl number and diameter ratio effects on natural convection heat transfer in horizontal cylindrical annuli was investigated by Kuehn and Goldstein [2]. They covered the ranges ($0.001 \le Pr \le 10^3$) and ($1 \le RR \le \infty$) to determine their influence on the flow and local and mean heat transfer in the annulus. As $Pr \to 0$, the temperature distribution approached the pure conduction limit. For $Pr \ge 1$, the temperature profiles are almost independent of *Pr* with thermal boundary layers adjacent to both cylinders. The distribution of the local *Nu* on the inner cylinder at large Pr resembles that on a single horizontal cylinder in boundary layer flow. Boyd [10] presented a correlation theory for natural convection data for horizontal annuli of arbitrary cross-section with application to concentric circular cylinders. It predicts local and mean heat transfer for $1.5 \le RR \le 3$ and $0.7 \le Pr \le 3100$. Mahony et al. [11] numerically investigated the variable property effects of gases in horizontal annuli in the range $1.5 \le RR \le 5$. Velocity and temperature profiles as well as heat transfer rates have been reported for temperature difference ratios $(T_h - T_c) / T_c$ from 0.2 to 0.3. They found that the Boussinesq approximation is valid for temperature difference ratios up to 0.2. The stability of the natural convection flow in the horizontal annulus was numerically studied by Cho and Kim [12]. For $1.2 \le RR \le 1.95$, the basic two –dimensional flow was found to be unstable with respect to three-dimensional disturbances and instability was mainly due to buoyancy effects. Rao et al. [13] investigated both numerically and experimentally the various flow patterns of natural convection in horizontal cylindrical annuli for *Pr* = 0.7 and 5000. They found different types of flow (stable or oscillatory) according to the values of *Ra* and *RR*. Yoo et al. [14] studied the flow patterns in a wide range of gap widths for *Pr* = 0.02. For low *Gr*, a steady unicellular flow was obtained. Above a transition value of *Gr* depending on the value of *RR*, a steady bicellular flow occurred. Yoo [15] extended the work for $Pr \le 0.3$ where steady or oscillatory flows consisting of multiple like-rotating cells were found for $Pr \le 0.2$. For $Pr = 0.3$, a counter-rotating cell on the top of the annulus was observed. For $Pr \cong 0$, the multiple cells were distributed uniformly in the lower and upper parts of the annulus. Bifurcation phenomena and existence of dual solutions in the annulus were numerically investigated by Yoo [16] for fluids of $0.3 \le Pr \le 1$. When the Rayleigh number exceeded a critical value, two kinds of flow patterns were realized: the first is the crescent-shaped eddy patterns in which the fluid in the top of the annulus ascends, and the second is the flow in which the fluid descends by forming two counter-rotating eddies in a half annulus.

2. Mathematical analysis

The steady-state dimensionless equations for the two-dimensional laminar free convection in cylindrical coordinates (r,ϕ) including the Boussinesq approximation are given by:

$$\frac{\partial V_r}{\partial R} + \frac{V_r}{R} + \frac{\partial V_\phi}{R\partial\phi} = 0, \tag{1}$$

$$\left(V_r \frac{\partial V_r}{\partial R} + V_\phi \frac{\partial V_r}{R\partial\phi} - \frac{V_\phi^2}{R} \right) = -\frac{\partial P_d}{\partial R} - \frac{Ra}{8\,Pr}\theta\cos\phi + \left(\frac{\partial^2 V_r}{\partial R^2} + \frac{1}{R}\frac{\partial V_r}{\partial R} - \frac{V_r}{R^2} + \frac{\partial^2 V_r}{R^2\partial\phi^2} - \frac{2}{R^2}\frac{\partial V_\phi}{\partial\phi} \right), \tag{2}$$

$$\left(V_r \frac{\partial V_\phi}{\partial R} + V_\phi \frac{\partial V_\phi}{R\partial\phi} + \frac{V_r V_\phi}{R} \right) = -\frac{\partial P_d}{R\partial\phi} + \frac{Ra}{8\,Pr}\theta\sin\phi + \left(\frac{\partial^2 V_\phi}{\partial R^2} + \frac{1}{R}\frac{\partial V_\phi}{\partial R} - \frac{V_\phi}{R^2} + \frac{\partial^2 V_\phi}{R^2\partial\phi^2} + \frac{2}{R^2}\frac{\partial V_r}{\partial\phi} \right), \tag{3}$$

$$\left(V_r \frac{\partial \theta}{\partial R} + V_\phi \frac{\partial \theta}{R \partial \phi}\right) = \frac{1}{Pr}\left[\frac{1}{R}\frac{\partial}{\partial R}\left(R\frac{\partial \theta}{\partial R}\right) + \frac{\partial^2 \theta}{R^2 \partial \phi^2}\right]. \quad (4)$$

The following dimensionless variables are used:

$$V_r = \frac{v_r}{(\nu/a)}, \quad V_\phi = \frac{v_\phi}{(\nu/a)}, \quad R = \frac{r}{a},$$
$$\theta = \left(\frac{T - T_c}{T_h - T_c}\right), \quad P_d = \frac{p_d}{\rho(\nu/a)^2}$$
$$Pr = \frac{Cp\mu}{k}, \quad Ra = \frac{(2a)^3 \beta g (T_h - T_c)}{\nu\alpha}, \quad RR = r_o / r_i. \quad (5)$$

The above equations are subjected to the following boundary conditions:

at $R = 1$ and $0 \le \phi \le \pi$, $V_r = 0$, $V_\phi = 0$, $\theta = 1$, (6-a)

at $R = RR$ and $0 \le \phi \le \pi$, $V_r = 0$, $V_\phi = 0$, $\theta = 0$, (6-b)

at $1 \le R \le RR$ and $\phi = 0$ or π, $V_\phi = 0$,
$$\frac{\partial V_r}{\partial \phi} = 0, \quad \frac{\partial \theta}{\partial \phi} = 0. \quad (6\text{-c})$$

The solution is obtained for only half of the annular gap because of the symmetry condition about the vertical axis. The solution domain and boundary conditions are shown in fig. 1.

2.1. Nusselt number calculation

The local Nusselt number, Nu_ϕ on the inner hot cylinder is defined as:

$$Nu_\phi = \frac{h_\phi (2a)}{k} = -2\frac{\partial \theta}{\partial R}\Big|_{R=1}, \quad (7)$$

and the average Nusselt number, Nu over the inner hot cylinder perimeter is given as:

$$Nu = \frac{h(2a)}{k} = \frac{-2}{\pi}\int_0^\pi \frac{\partial \theta}{\partial R} d\phi = \frac{-2}{\pi}\sum_0^\pi \left(\frac{\partial \theta}{\partial R}\right)_{R=1} \Delta\phi. \quad (8)$$

2.2. Grid system

The grid system of the half annular space consists of 50 nodes in the radial direction with non-uniform spacing. The nodes are denser near the inner and outer cylinder surfaces and coarser away from them. In the circumferential direction, 90 nodes were taken with uniform spacing.

2.3. Numerical solution

The finite difference technique developed by Patankar [17] is used to solve the governing eqs. (1-4) with their boundary conditions given in eqs. (6-a, 6-b and 6-c). The discretized equations used central differencing in space and were solved by Gauss-seidel elimination method. A line by line procedure is used in the iterations. The continuity and momentum equations are first solved simultaneously and then the energy equation. The solution was stopped when the change in the average Nusselt number over 100 iterations is less than 0.01 % of its value. 1500 iterations were quite enough to reach the required accuracy in most of the runs.

The governing equations were casted in the following general form of the transport equation used by Patankar [17] for steady state in (r-ϕ) cylinder coordinates.

$$\frac{1}{r}\frac{\partial}{\partial r}\left[r\left(\rho V_r \phi^* - \Gamma \frac{\partial \phi^*}{\partial r}\right)\right] + \frac{1}{r}\frac{\partial}{\partial \phi}\left[\rho V_\phi \phi^* - \Gamma \frac{\partial \phi^*}{r \partial \phi}\right] = S_C + S_V . \phi^*. \quad (9)$$

Where:

ϕ^* is the transported quantity into consideration,

Γ is the diffusion coefficient of ϕ^*,

S_C is the constant part of the source term of ϕ^*, and

S_V is the variable part of the source term of ϕ^*.

The results for the diffusion coefficients and source terms for the four governing equations are summarized in table 1.

Table 1
Dimensionless diffusion coefficients and source terms for the governing equations

ϕ^*	ρ	Γ	S_C	S_V
1	1	0	0	0
V_r	1	1	$-\frac{\partial P_d}{\partial R}-\frac{Ra}{8\,Pr}\theta\cos\phi+\frac{V_\phi^2}{R}-\frac{2}{R^2}\frac{\partial V_\phi}{\partial\phi}$	$-\frac{1}{R^2}$
V_ϕ	1	1	$-\frac{\partial P_d}{R\partial\phi}+\frac{Ra}{8\,Pr}\theta\sin\phi+\frac{2}{R^2}\frac{\partial V_r}{\partial\phi}$	$-\frac{V_r}{R}-\frac{1}{R^2}$
θ	1	$\frac{1}{Pr}$	0	0

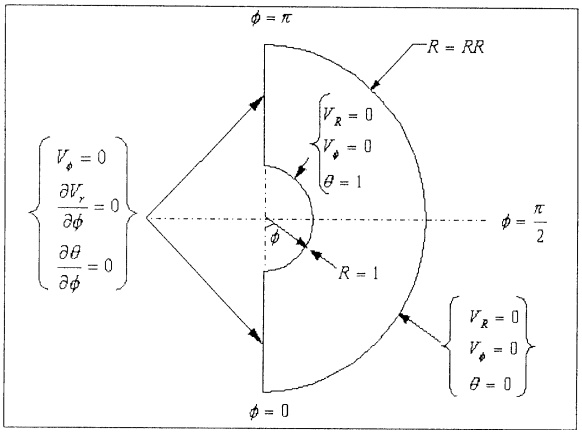

Fig.1. Solution domain and boundary conditions.

3. Results

3.1. Streamlines

The effects of *Pr* on the flow in the horizontal annulus can be explained from the streamlines and isotherms at different values of *Pr* and fixed values of *RR* and *Ra*. Fig. 2 shows the streamlines for *RR*=2 and *Ra*=10^2. At this low value of *Ra*, steady unicellular flow in the form of a crescent-shape eddy is observed which indicates the pure conduction regime. The fluid rises near the inner hot cylinder and sinks near the outer cold cylinder. As *Pr* was increased from 0.01 to 10, the stream function was reduced indicating continuous reduction in the flow velocity. However, the conduction regime prevails. For *Ra*=10^6 and *RR*=2, several counter-rotating eddies as shown in fig. 3 were formed with high rotating velocities at low *Pr* (*Pr* = 0.01). As *Pr* was increased to 0.1, only two counter-rotating cells were observed with lower rotating velocities. For *Pr* ≥ 1, the flow velocity continued to reduce and a steady flow of the crescent-shape was observed with its center of rotation moving upward in the cavity as *Pr* was increased.

To show the effect of radius ratio on the flow, a wide cavity with *RR*=10 was investigated. For *Ra*=10^2, fig. 4 shows the streamlines as counter-rotation cells for *Pr* =0.01. For *Pr* ≥ 0.1, the steady unicellular flow existed with its center of rotation moving upward as *Pr* was increased. When *Ra* was increased to *Ra*=10^6, the flow for *Pr* =0.01 was similar to that on a single horizontal cylinder as shown in fig. 5. For *Pr* ≥ 0.1, the boundary layer flow existed with a thermal boundary layer adjacent to each cylinder.

3.2. Isotherms

For *RR*=2 and *Ra*=10^2, fig. 6 shows the isotherms as concentric cylinders for 0.01 ≤ *Pr* ≤ 10 which indicates pure conduction in the annulus. For *RR*=2 and *Ra*=10^6 , the boundary layer flow existed , as shown in fig. 7, with isotherms moving closer to the bottom of the inner cylinder and the top of the outer one as *Pr* was increased . For the wide cavity of *RR*=10 and *Ra*=10^2 , a transition from the conduction regime at low *Pr* to the boundary layer regime is noticed as shown in fig. 8. For *Ra*=10^6, fig. 9 shows isotherms confined to the inner cylinder for *Pr*=0.01 as in the case of a single cylinder. For *Pr* ≥ 0.1, the thermal boundary layers are shown close to each cylinder with stratified flow in the core of the cavity.

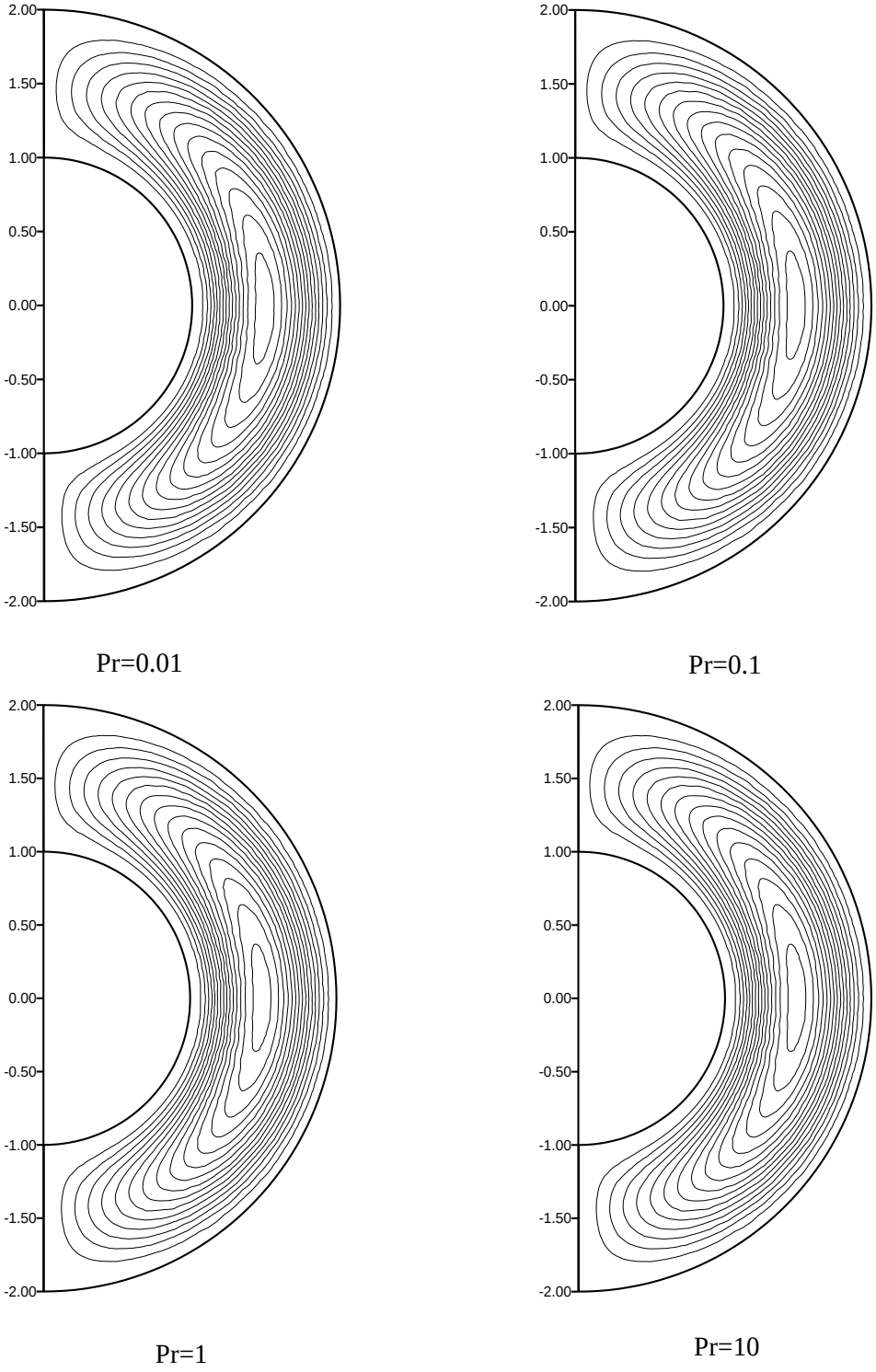

Fig. 2. Streamlines for *RR*=2, *Ra* = 10^2.

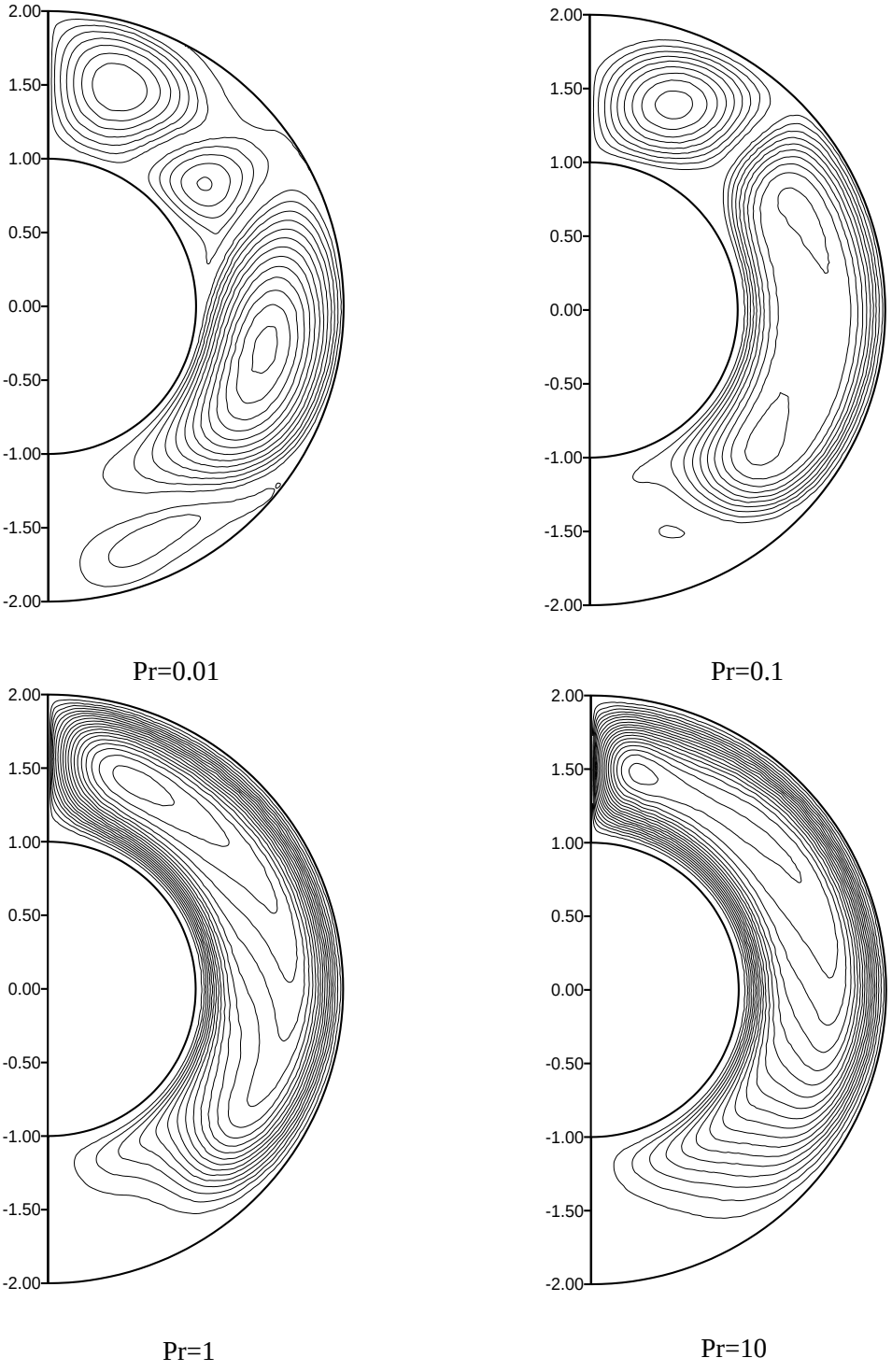

Fig. 3. Streamlines for *RR*=2, *Ra* = 10^6.

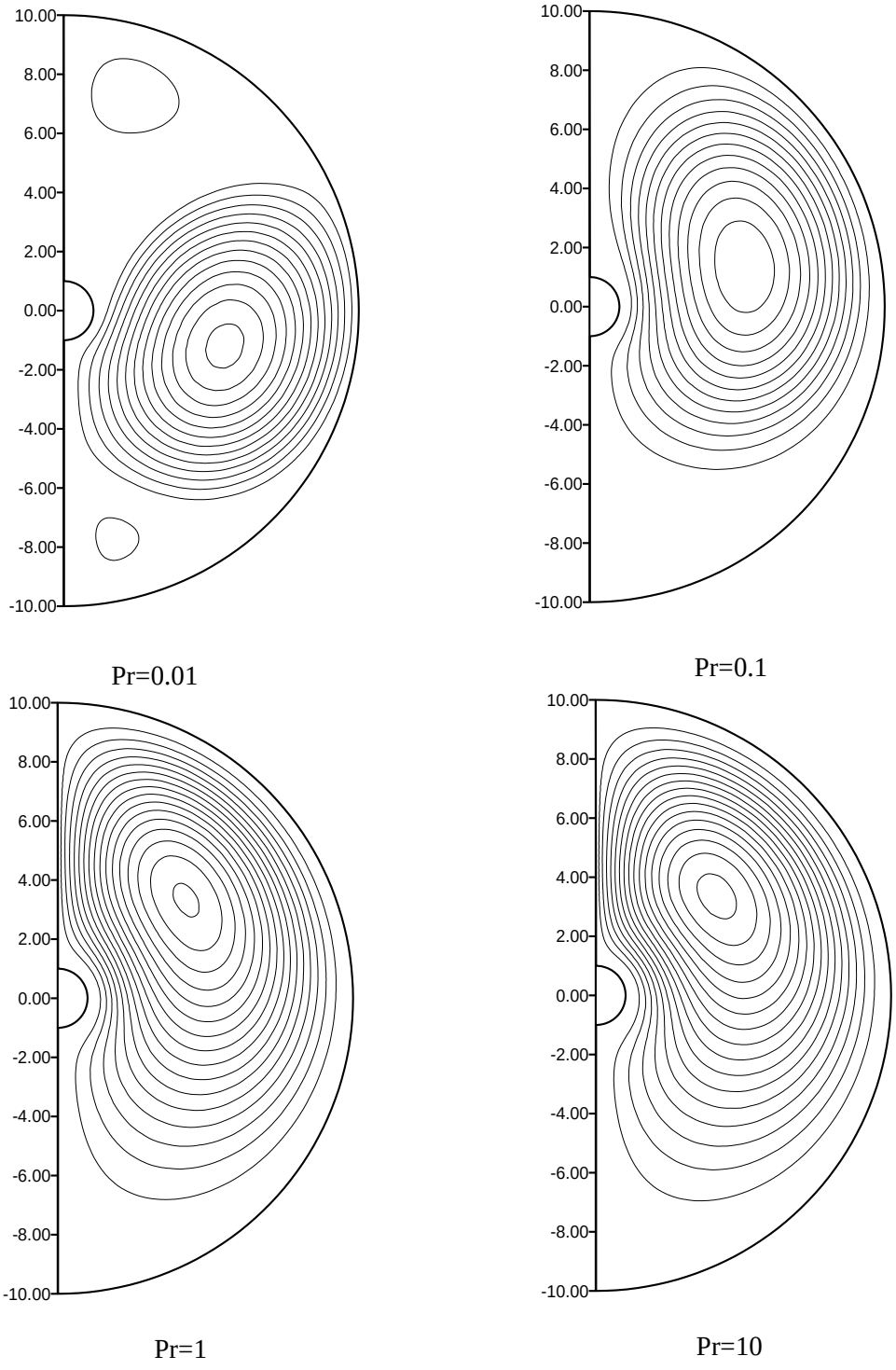

Fig. 4. Streamlines for RR=10, Ra = 10^2.

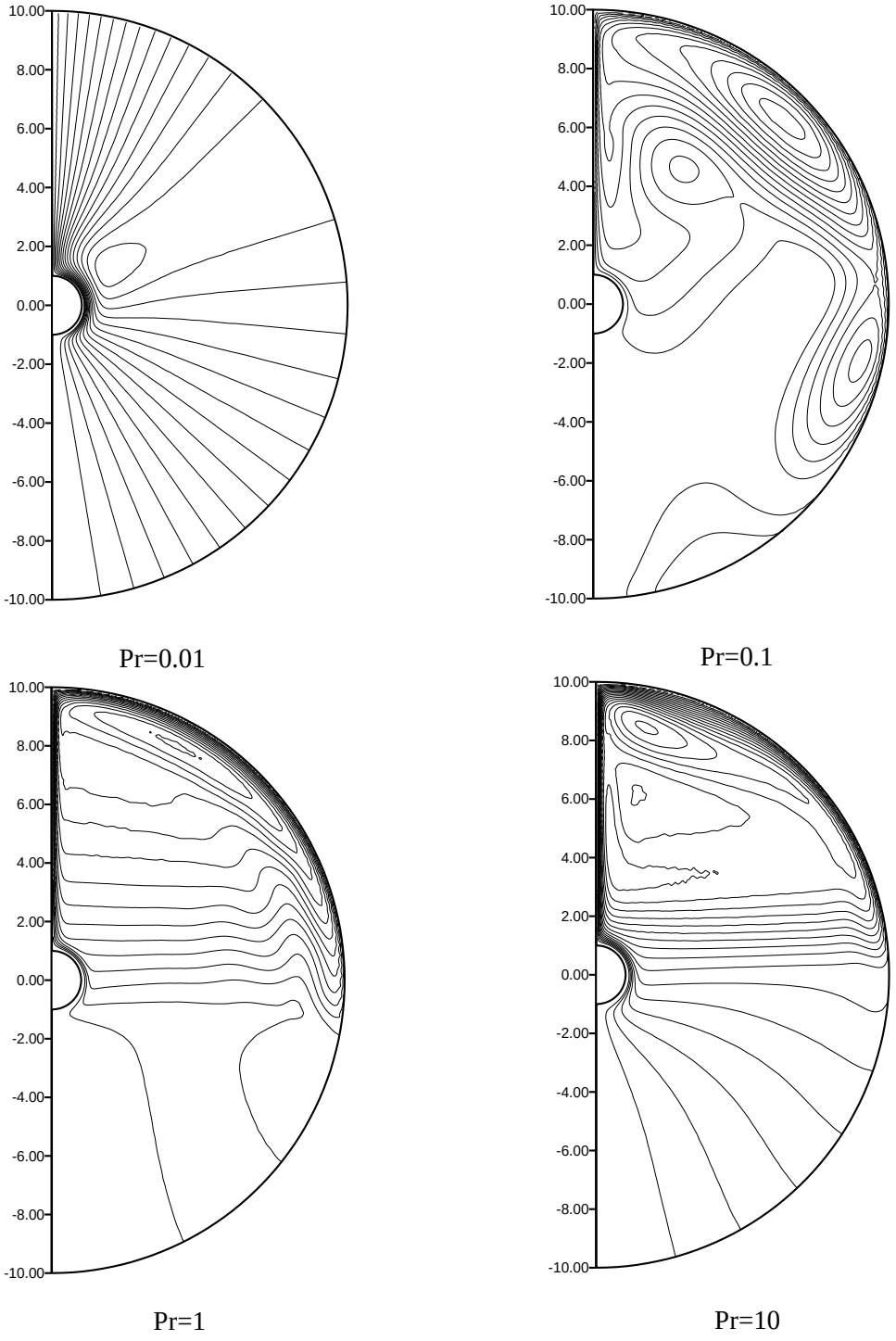

Fig. 5. Streamlines for RR=10, Ra = 10^6.

3.3. Average Nusselt number

The effects of Pr on the Nusselt number are shown in figs. 10, 11. For RR=2, as in fig. 10, the conduction regime persists for $Ra \leq 10^4$ with a constant value of Nu close to the conduction limit (Nu_{con}=2 / ln RR) . For $Ra > 10^4$, the average Nusselt number increased with Ra with higher increase for higher Pr. For $Pr \geq 1$, no significant effect on Nu was shown. For RR=10, fig. 11 shows continuous increase in Nu with both Ra and Pr. For $Pr \geq 10^2$, the average Nusselt number did not change with Pr.

3.4. Local Nusselt number

The local Nusselt number distributions at the inner hot cylinder are shown in figs. 12, 13. For RR=2 and Ra=10^6, the local Nusselt number for Pr=0.01 is high at the cylinder bottom (ϕ =0) and gradually decreases till $\phi \cong 120^o$ where separation of the flow occurs. It starts to increase again up to $\phi \cong 150^o$ and then decreases up to the top of the cylinder. This behaviour continues for low Pr up to $Pr \cong$ 0.1. For $Pr \geq 0.7$, a monotonic decrease in local Nusselt occurs from the bottom to the top of the inner cylinder.

For RR=10 and Ra=10^6, fig. 13 shows a gradual decrease in local Nusselt number for all values of Pr. However, for low Pr ($Pr \leq 0.1$) separation of flow occurs near the top of the cylinder at $\phi \cong 170^o$.

3.5. Angular velocity and temperature distributions

The distribution of the angular velocity, V_ϕ along a radius at $\phi \cong 90^o$ is shown in fig. 14-a for RR=2, Ra=10^6 and $0.01 \leq Pr \leq 10^3$. The velocity increases from zero at inner cylinder wall to a maximum in the upwards direction and then gradually drops to zero at the middle of the cavity. In the outer half of the annulus, the angular velocity increases in the downwards direction and then it is reduced to stagnation at the outer cylinder wall. The maximum value of V_ϕ increases with Pr and shifts closer to the cylinder walls as Pr was increased.

The distribution of the temperature along a radius at ϕ =90^o for RR=2, Ra=10^6 and $0.01 \leq Pr \leq 10^3$ is given in fig. 14-b. A continuous decrease along the radius is shown with higher changes near the cylinder walls. A slight reverse in the temperature slope is shown in the core of the cavity which is a characteristic of the boundary layer type of flow shown in fig. 7. This temperature inversion phenomenon has also been shown previously both numerically [4,8,11] and experimentally[1]. No further change was noticed for $Pr \geq 10$.

4. Correlations

The average Nusselt number over the inner hot cylinder for natural convection in horizontal fluid annular cavities was correlated using the method suggested by Churchill and Chu [18]. Using a Least-squares method, the correlations are given as:

$$Nu = \left(Nu_{cond}{}^{15} + Nu_{conv}{}^{15}\right)^{1/15}, \qquad \text{(10-a)}$$

where,

$$Nu_{cond} = \frac{2}{Ln(RR)}, \qquad \text{(10-b)}$$

$$Nu_{conv} = \frac{2}{Ln\left[\dfrac{1+\dfrac{2}{0.3579\,(Ra)^{0.294}\left[1+\left(\dfrac{9.96\times10^{-4}}{Pr}\right)^{0.39}\right]^{-2.36}}}{1-\dfrac{2}{0.8195\left(Ra.RR^3\right)^{0.206}}}\right]}. \qquad \text{(10-c)}$$

The above correlation is valid for the ranges $1.25 \leq RR \leq 10$, $10^2 \leq Ra \leq 10^6$ and $0.01 \leq Pr \leq 10^3$. The average deviation in the numerical results from the correlation is 3.4 % and the standard deviation is about 0.014.

5. Conclusions

The effects of the Prandtl numbers on laminar flow and heat transfer in fluid layers

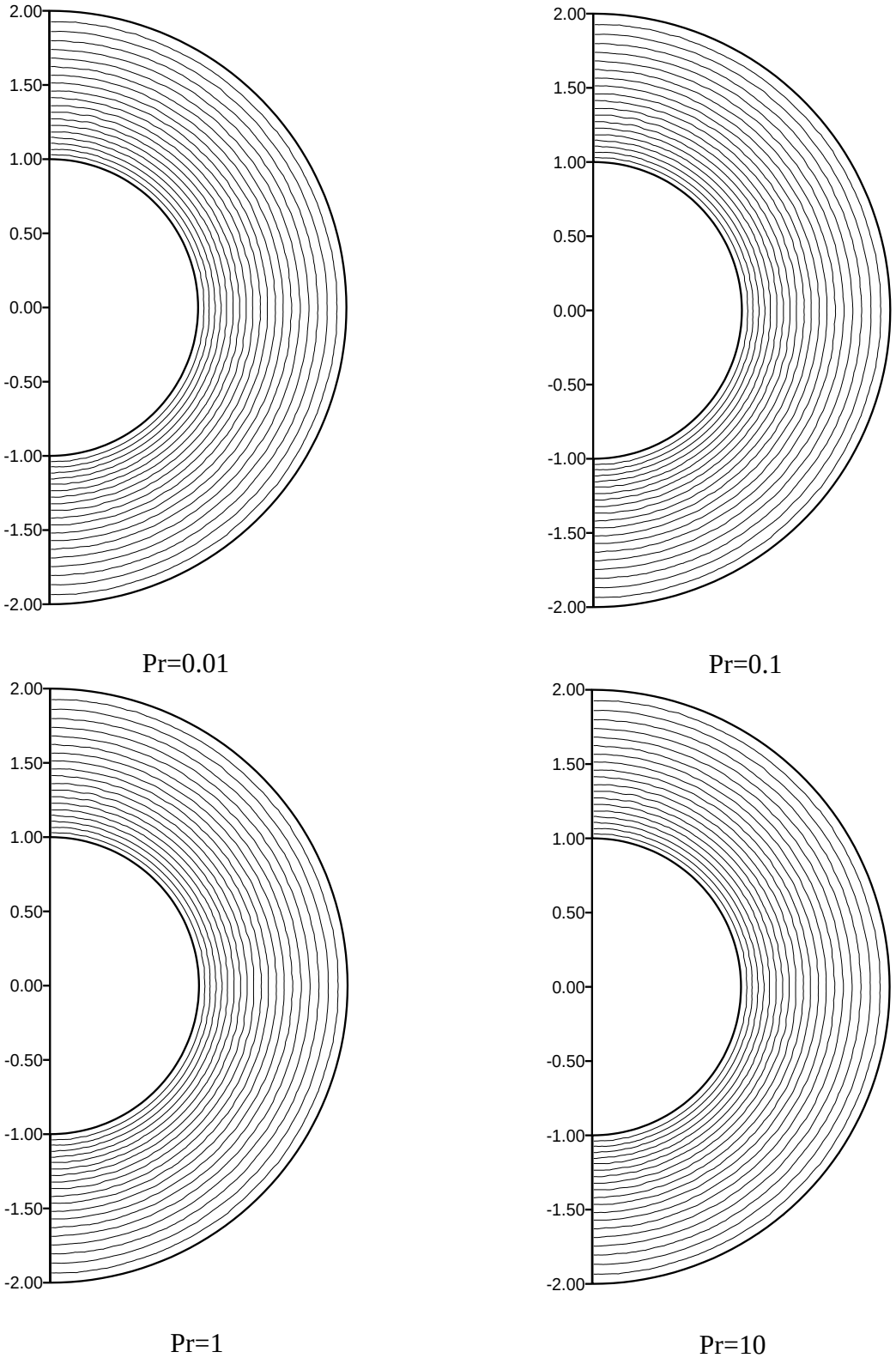

Fig. 6. Isotherms for RR=2, Ra = 10^2.

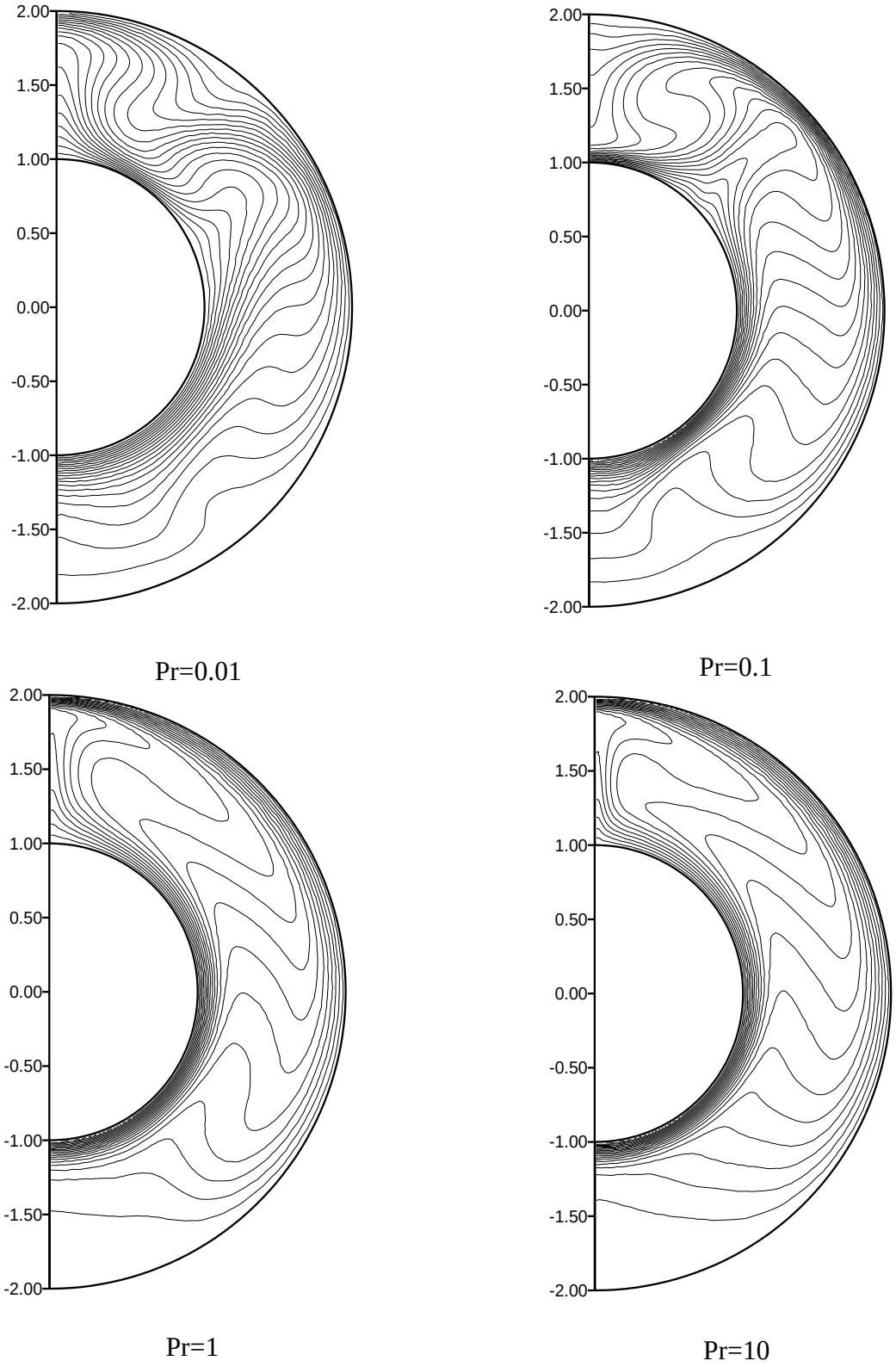

Fig. 7. Isotherms for RR=2, Ra = 10^6.

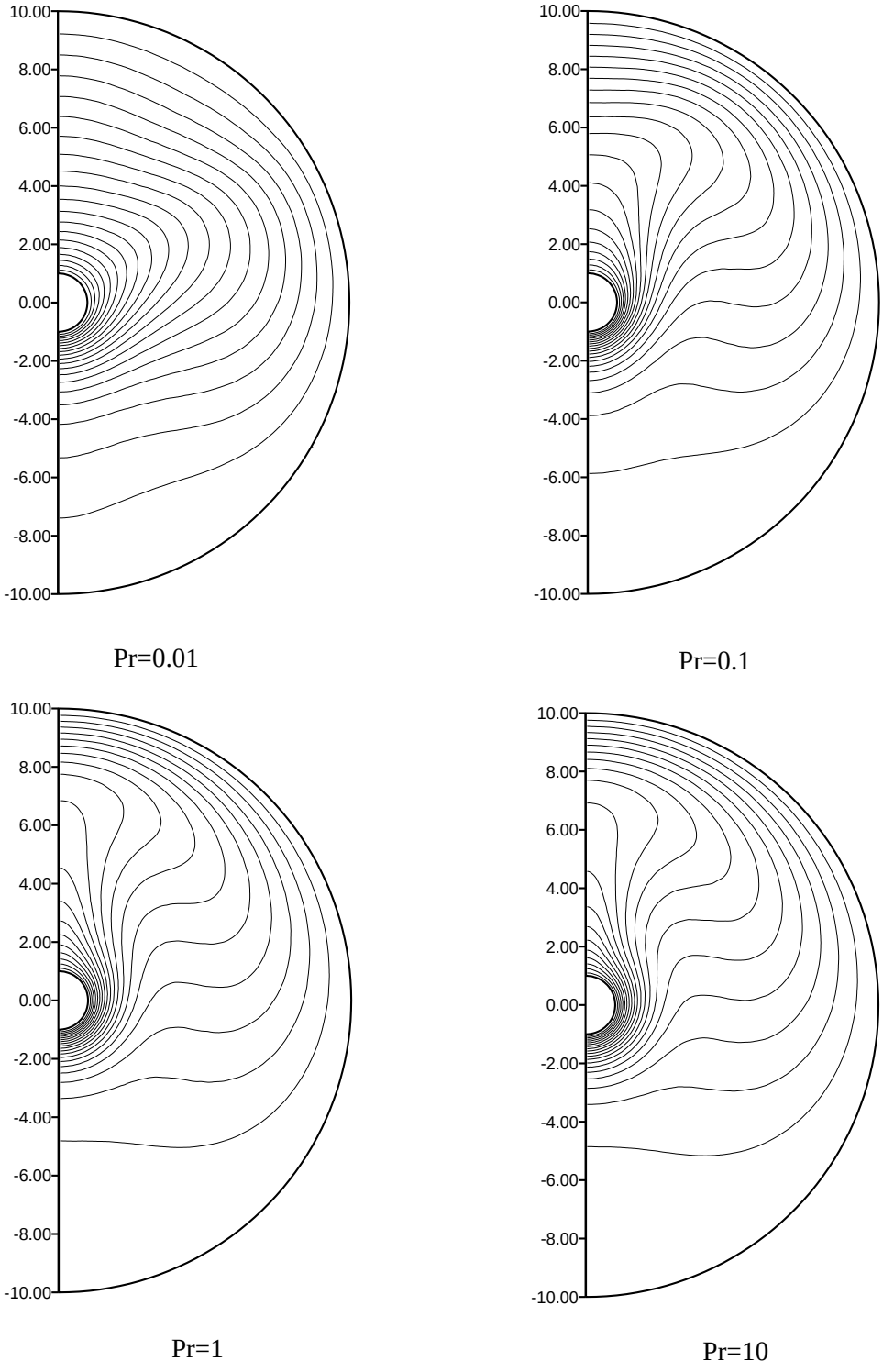

Fig. 8. Isotherms for *RR*=10, *Ra* = 10^2.

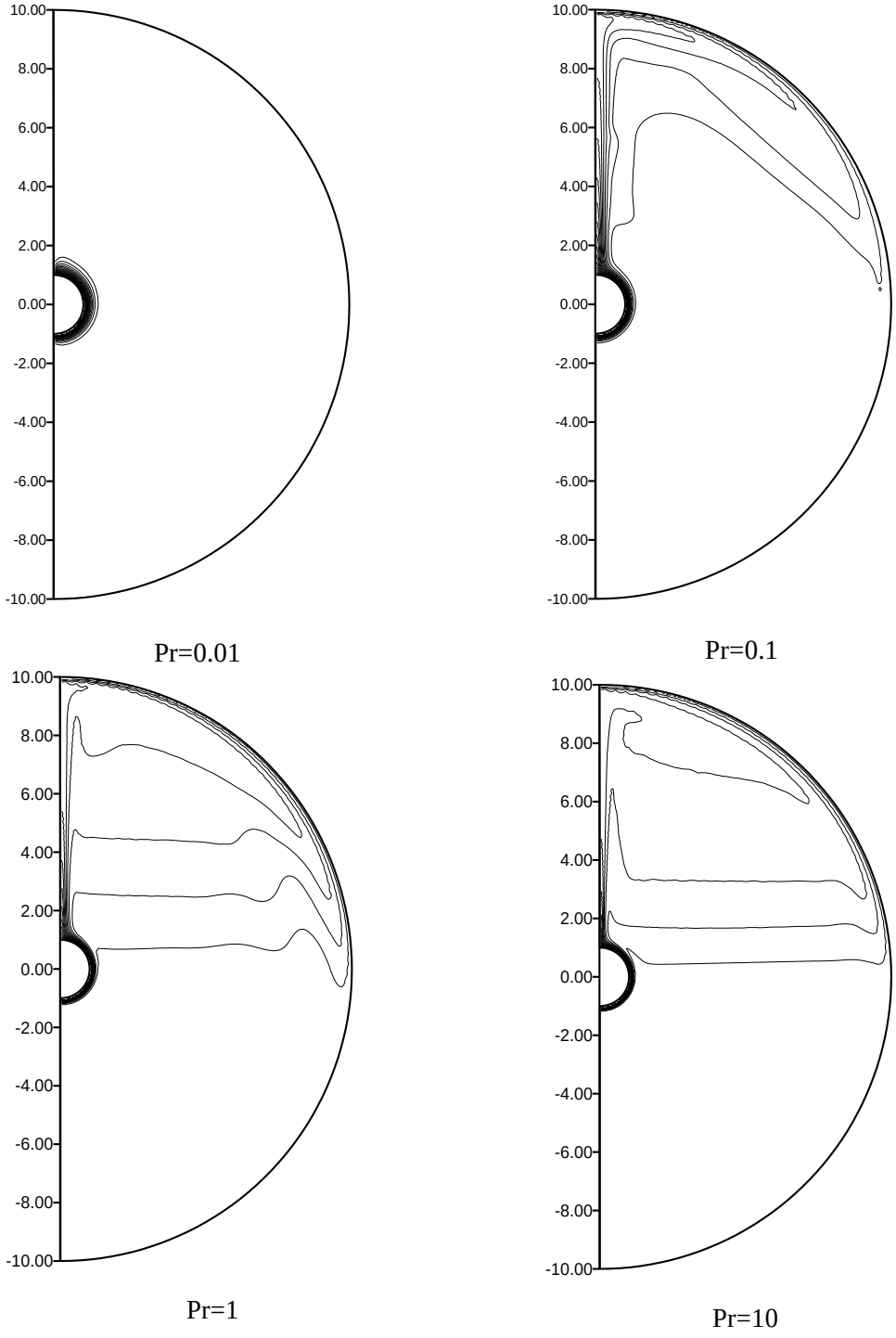

Fig. 9. Isotherms for *RR*=10, *Ra* = 10^6.

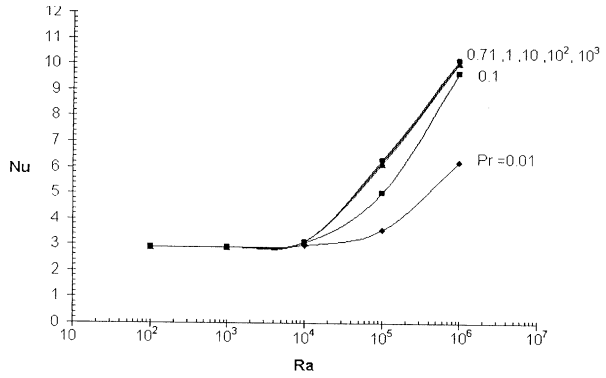

Fig. 10. Average Nusselt number for *RR*=2.

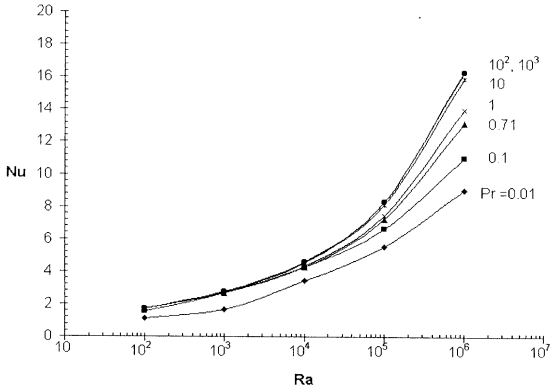

Fig. 11. Average Nusselt number for *RR*=10.

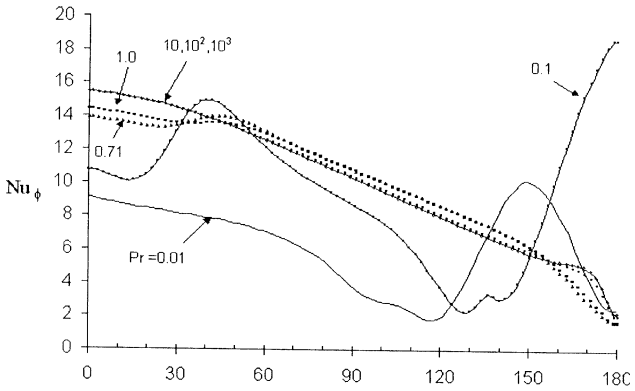

Fig. 12. Local Nusselt number distribution for *RR*=2 and *Ra*=10⁶.

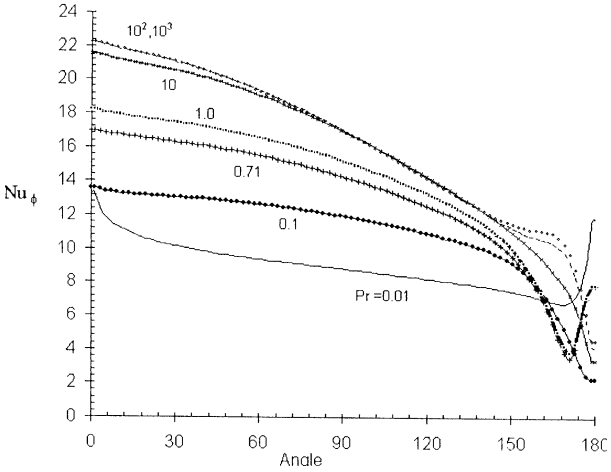

Fig. 13. Local Nusselt number distribution for *RR*=10 and *Ra*=10⁶.

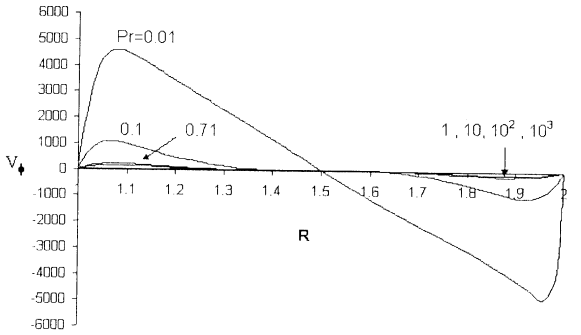

(a) Angular velocity component

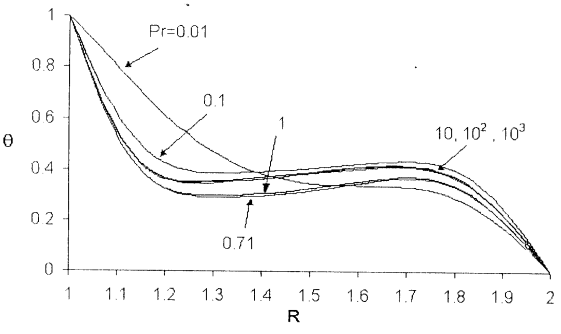

(b) Temperature distribution

Fig. 14. Velocities and Temperature distributions along a radius for *RR*=2, ϕ = 90°, *Ra* = 10⁶.

contained between isothermal concentric horizontal cylinders are investigated. The study covered the ranges $0.01 \le Pr \le 10^3$, $1.25 \le RR \le 10$ and $10^2 \le Ra \le 10^6$. Streamlines and isotherms are presented to explain the flow regime at different values of the studied parameters. For RR=2, the conduction regime prevails for all Pr up to Ra =10^4, then the boundary layer regime started with higher heat transfer at higher Pr. For RR =10, the boundary layer regime was found for $Ra \ge 10^2$ and all Pr. Local and average Nu numbers are given for all Pr and for RR =2 and 10 . The general effect of Pr was to increase Nu as Pr was increased for the boundary layer regime. Separation of the flow occurred near the inner cylinder top for low Pr. Angular velocity and temperature distributions are given to explain the flow regimes. A general correlation for Nu is given which represents all numerical results to within 3.4 %.

Nomenclature

a is the radius of inner hot cylinder , ($a = r_i$) , m.
c_p is the specific heat , J/kgK,
g is the gravitational acceleration , m/s^2,
Gr is the Grashof number, $g\beta(Th - Tc)(2a)^3/\nu^2$,
h average heat transfer coefficient, W/m^{2}K,
h_ϕ is the local heat transfer coefficient, W/m^{2}K,
k is the thermal conductivity, W/mK,
Nu is the average Nusselt number, $h(2a)$/k,
Nu_ϕ is the local Nusselt number, $h_\phi (2a)$/k,
p_d is the dynamic pressure, N/m^2,
P_d is the dimensionless dynamic pressure, $P_d = \dfrac{p_d}{\rho(\nu/a)^2}$,
Pr is the Prandtl number, μc_p/k,
r is the radial coordinate, m
r_i is the radius of inner cylinder, m,
r_o is the radius of outer cylinder, m,
R is the dimensionless radial coordinate, r/a,
RR is the radius ratio, r_o/r_i,
Ra is the Rayleigh number based on inner diameter, $g\beta(T_h - T_c)(2a)^3/\nu\alpha$,
T is the local fluid temperature, K,
v_r is the radial velocity , m/s ,
V_r is the dimensionless radial velocity,
v_ϕ is the angular velocity, m/s, and
V_ϕ is the dimensionless angular velocity.

Greek symbols

α is the thermal diffusivity, $K/c_p\rho$, m^2/s,
β is the coefficient of volumetric thermal expansion, K^{-1},
ρ is the local density, kg/m^3,
μ is the dynamic viscosity, kg/ms,
ν is the kinematic viscosity , μ/ρ, m^2/s,
ϕ is the angular coordinate, rad, and
θ is the dimensionless temperature , $(T-T_c)$ / $(T_h - T_c)$.

Subscripts

c is the cold,
$cond$ is the conduction,
$conv$ is the convection,
h is the hot,
i is the inner, and
o is the outer.

References

[1] T.H. Kuehn and R.J. Goldstein, "An Experimental And Theoretical Study of Natural Convection in the Annulus Between Horizontal Concentric Cylinders" , J. Fluid Mech. , Vol. 74 (4), pp. 695-719 (1976).

[2] T.H. Kuehn and R.J. Goldstein, "A Parametric Study of Prandtl Number And Diameter Ratio Effects on Natural Convection Heat Transfer in Horizontal Cylindrical Annuli" , J. Heat Transfer, Vol. 102, pp. 768-770 (1980).

[3] T.H. Kuehn and R.J. Goldstein, "Correlating Equations for Natural Convection Heat Transfer Between Horizontal Circular Cylinders", Int. J. Heat Mass Transfer, Vol. 19, pp. 1127-1134 (1976).

[4] C.H. Cho, K.S. Chang and K.H. Park, "Numerical Simulation Of Natural Convection in Concentric and Eccentric Horizontal Cylindrical Annuli", J. Heat Transfer, Vol. 104, pp. 624-630 (1982).

[5] U. Grigull and W. Hauf, "Natural Convection in Horizontal Cylindrical Annuli", Proc. of the Third Int. Heat Transfer Conf., Illinois, Vol. 2, pp. 182-195 (1966).

[6] J. Lis, "Experimental Investigation of Natural Convection Heat Transfer in Simple and Obstructed Horizontal Annuli", proc. of the third Int. Heat Transfer Conf., Illinois, Vol. 2, pp. 196-204 (1966).

[7] B. Farouk and S.I. Güceri, "Laminar and Turbulent Natural Convection in the Annulus Between Horizontal Concentric Cylinders", J. Heat Transfer, Vol. 104, pp. 631-636 (1982).

[8] M.A. Hessami, A. Pollard and R.D. Rowe, "Numerical Calculation of Natural Convective Heat Transfer Between Horizontal Concentric Isothermal Cylinders- Effects of the Variation of the Fluid Properties", ASME J. Heat Transfer, Vol. 106, pp. 668-671(1984).

[9] M.A. Hessami, A. Pollard, R.D. Rowe and D.W. Ruth, "A Study of Free Convective heat Transfer in a Horizontal Annulus With a Large Radii Ratio", J. Heat Transfer, Vol. 107, pp. 603-610 (1985).

[10] R.D. Boyd, "A Correlation Theory for Steady Natural Convective Heat Transport in Horizontal Annuli", J. Heat Transfer, Vol. 105, pp. 144-150 (1983).

[11] D.N. Mahony, R. Kumar and E.H. Bishop, "Numerical Investigation of Variable Property Effects on Laminar Natural Convection of Gases Between Two Horizontal Isothermal Concentric cylinders", J. Heat Transfer, Vol. 108, pp. 783 –789 (1986).

[12] J.Y. Choi and M.U. Kim, "Three-Dimensional Linear Stability of Natural Convection Flow Between Concentric Horizontal Cylinders", Int. J. Heat Mass Transfer, Vol. 36 (17), pp. 4173-4180 (1993).

[13] Y.F. Rao, Y. Miki, K. Fukuda, Y. Takata and S. Hasegawa, "Flow Patterns of Natural Convection in Horizontal Cylindrical Annuli", Int. J. Heat Mass Transfer, Vol. 28 (3), pp. 705-714 (1985).

[14] J.S. Yoo, J.Y. Choi and M.U. Kim, "Multicellular Natural Convection of a Low Prandtl Number Fluid Between Horizontal Concentric Cylinders", Num. Heat Transfer, Part A, Vol. 25, pp. 103-115 (1994).

[15] J.S. Yoo, "Natural Convection in a Narrow Horizontal Cylindrical Annulus: $Pr \leq 0.3$", Int. J. Heat Mass Transfer, Vol. 41, pp. 3055-3073 (1998).

[16] J.S. Yoo, "Prandtl Number Effect on Bifurcation and Dual Solutions in Natural Convection in a Horizontal Annulus", Int. J. Heat Mass Transfer, Vol. 42 , pp. 3279-3290 (1999).

[17] S.V. Patankar, Numerical Heat Transfer and Fluid Flow, Mc Graw- Hill , New York (1980).

[18] S.W. Churchill and H.H.S. Chu, "Correlating Equations for Laminar and Turbulent free Convection from a Horizontal Cylinder", Int. J. Heat Mass Transfer, Vol. 18, pp. 1049-1053 (1975).

Received June 22, 2004
Accepted August 31, 2004